Signatures of low-dimensional magnetism and short-range magnetic order in Co-based trirutiles

R. Baral,[1] H. S. Fierro,[1] C. Rueda,[1] B. Sahu,[2] A. M. Strydom,[2] N. Poudel,[3] K. Gofryk,[3] F. S. Manciu,[1] C. Ritter,[4] T. W. Heitmann,[5] B. P. Belbase,[6,7,*] S. Bati,[6,7,*] M. P. Ghimire,[6,8,7] and H. S. Nair[1,†]

[1]*Department of Physics, 500 W University Ave, University of Texas at El Paso, El Paso, Texas 79968, USA*
[2]*Highly Correlated Matter Research Group, Department of Physics, University of Johannesburg, P.O. Box 524, Auckland Park 2006, South Africa*
[3]*Idaho National Laboratory, Idaho Falls, Idaho 83415, USA*
[4]*Institut Laue Langevin, 71, Avenue des Martyrs, Grenoble 38000, France*
[5]*University of Missouri Research Reactor, University of Missouri, Columbia, Missouri 65211, USA*
[6]*Central Department of Physics, Tribhuvan University, Kirtipur, 44613, Kathmandu, Nepal*
[7]*Condensed Matter Physics Research Center, Butwal, Rupandehi, Nepal*
[8]*Leibniz Institute for Solid State and Materials Research IFW Dresden, 01069 Dresden, Germany*

(Received 12 August 2019; revised manuscript received 17 October 2019; published 6 November 2019)

Features of low-dimensional magnetism resulting from a square-net arrangement of Co atoms in trirutile $CoTa_2O_6$ are studied in the present work by means of density functional theory and are compared with the experimental results of specific heat and neutron diffraction. The small total energy differences between the ferromagnetic (FM) and antiferromagnetic (AFM) configuration of $CoTa_2O_6$ shows that competing magnetic ground states exist, with the possibility of transition from FM to AFM phase at low temperature. Our calculation further suggests the semiconducting behavior for $CoTa_2O_6$ with a band gap of ~0.41 eV. The calculated magnetic anisotropy energy is ~2.5 meV with its easy axis along the [100] (in-plane) direction. Studying the evolution of magnetism in $Co_{1-x}Mg_xTa_2O_6$ ($x = 0$, 0.1, 0.3, 0.5, 0.7, and 1), it is found that the sharp AFM transition exhibited by $CoTa_2O_6$ at $T_N = 6.2$ K in its heat capacity vanishes with Mg dilution, indicating the obvious effect of weakening the superexchange pathways of Co. The current specific heat study reveals the robust nature of T_N for $CoTa_2O_6$ in applied magnetic fields. Clear indication of short-range magnetism is obtained from the magnetic entropy, however, diffuse components are absent in neutron diffraction data. At T_N, $CoTa_2O_6$ enters a long-range ordered magnetic state which can be described using a propagation vector, $(\frac{1}{4}\frac{1}{4}0)$. Upon Mg dilution at $x \geqslant 0.1$, the long-range ordered magnetism is destroyed. The present results should motivate an investigation of magnetic excitations in this low-dimensional anisotropic magnet.

DOI: 10.1103/PhysRevB.100.184407

I. INTRODUCTION

$CoTa_2O_6$ belongs to the class of MT_2O_6 (M = Ni, Fe, Co; T = Ta, Sb) low-dimensional magnetic oxide compounds in trirutile structure. One of the earliest studies on $CoTa_2O_6$ reports a broad transition at 14 K in magnetization and relates it to low-dimensional physics [1]. Specific heat of $CoTa_2O_6$ was studied early on and was analyzed based on the model of an Ising net of spins, again making a connection to low dimensionality [2]. Subsequent studies by other groups have identified reduced dimensionality of magnetic interactions present in trirutiles that adopt the $P4_2/mnm$ space group where the transition metal is situated inside an octahedral environment produced by oxygen ligands. The magnetic superexchange pathways are dictated by the one dimensional M-O-O-M chains along [110] at $z = 0$ and $[1\bar{1}0]$ at $z = \frac{1}{2}$, which renders low dimensionality to the Co spin system [3,4]. The importance of this class of low-dimensional magnets has been put forward with respect to antiferromagnets with reduced dimensionality that can realize Luttinger liquids [5] and one-dimensional antiferromagnets in external magnetic fields that can realize spin liquids [6–9]. Strongly correlated magnetic behavior with reduced dimensionality has been seen in a related trirutile tantalate, $NiTa_2O_6$ [10]. Experimental and theoretical support for low dimensionality and anisotropic exchange interactions parallel and perpendicular to spin chains are found in several related systems [11–15].

Recent investigation on $CoTa_2O_6$ has revealed optical dichroism in the single crystals [16]. The dichroism was attributed to the anisotropic exchange mechanism related to the M-O-O-M chains. In addition to the low-dimensionality and anisotropic exchange, the specific heat of $CoTa_2O_6$ presented evidence for a large fraction of spins of Co remaining disordered even at very low temperatures below the T_N (6.1 K) [16]. The value of entropy change, 4.11 J/mol-K, was estimated to be below the maximum value for $S = 1/2$. However, this must be seen against a significant amount of entropy release in $CoTa_2O_6$ occurring above T_N. Effects of anisotropy are reported in the specific heat of $CoTa_2O_6$ measured with external magnetic field applied parallel and perpendicular to the spin chains of Co. When the applied field was parallel to [110], a broad peak emerged below the main peak at T_N.

*These authors contributed equally to this work.
†hnair@utep.edu

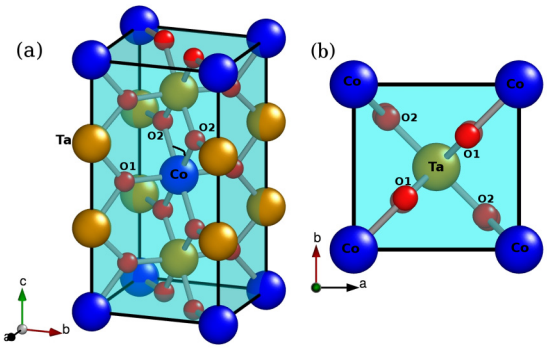

FIG. 1. The crystal structure of $CoTa_2O_6$. (a) The Co atoms represented by blue spheres form CoO_6 octahedra with the oxygen atoms (in red). (b) Shows a projection on to the *ab* plane from which the square planar arrangement of Co can be seen. The figures were created using the xfplo version of FPLO [17].

While the peak at T_N remained robust up to 8 T, the broad peak shifted its position under the application of field. On the other hand, when the field was parallel to [100], only one peak was detected in the specific heat. The anisotropy in magnetization and specific heat contributed towards a moderate magnetocaloric effect in $CoTa_2O_6$ [16]. An anisotropic magnetocaloric effect has been reported in $NiTa_2O_6$ [12]. Spin-phonon interactions and their signatures in low-dimensional magnetic systems were recently probed in the case of MT_2O_6 (M = Ni, Co; T = Ta, Sb) [18]. Significant reduction in the thermal conductivity of the Ta-based compounds was observed compared to that of the Sb-based systems. The thermal conductivity in these compounds was described based on resonant absorption of phonons in a two-level system. In order to clearly understand the connection between the spin and lattice entities, an unambiguous determination of the crystal and magnetic structures is a prerequisite.

Existing reports on the magnetic structure of $CoTa_2O_6$ describe slightly differing structures [3,19,20]. The most recent estimation of magnetic structure is that of an antiferromagnetic structure with the propagation vector $(\pm\frac{1}{4}\ \frac{1}{4}\ \frac{1}{4})$ where the magnetic moments lie entirely on the Co-O planes leading to a two-dimensional magnetic structure [20]. In an earlier study of the solid solution $Fe_xCo_{1-x}Ta_2O_6$ using neutron diffraction, a double-k magnetic structure with $(\pm\frac{1}{4}\ \frac{1}{4}\ \frac{1}{4})$ was reported for $CoTa_2O_6$ while $FeTa_2O_6$ had $(\frac{1}{2}\ 0\ \frac{1}{2})$ and $(0\ \frac{1}{2}\ \frac{1}{2})$ [19]. This study pointed out the existence of a bicritical point in the xT phase diagram of the mixed composition. One of the earliest neutron diffraction studies of $CoTa_2O_6$ had ascribed the observed magnetic reflections to a propagation vector $(\frac{1}{4}\ \frac{1}{4}\ \frac{1}{4})$ and used a two-cone axis helical spin structure to explain its magnetic structure [3]. In the present report, we extend our preliminary investigation using magnetization [21] to include a detailed study of the $Co_{1-x}Mg_xTa_2O_6$ compounds using neutron diffraction, specific heat, Raman scattering, thermal conductivity, and density functional theory computations. Our work provides support to the previous findings on low-dimensional magnetism but also improves the determination of the magnetic structure through neutron diffraction. The importance of inherent short-range spin dynamics is highlighted to warrant future neutron spectroscopic work (Fig. 1).

II. EXPERIMENTAL METHODS

The polycrystalline powder samples used in the present study were prepared following the prescriptions used in a previous work [21]. Neutron diffraction experiments were carried out on 4 g powders, at the PSD instrument in the University of Missouri Research Reactor (MURR) using $\lambda = 1.485$ Å. The sample powders were loaded in a vanadium can which was placed in an Al holder purged and filled with helium. Diffraction patterns were collected at different temperatures including 295 K, 7 K, and 5 K for different compositions. Fullprof suite of programs [22] was used to perform the Rietveld analysis [23] of the diffractograms. Determination of the magnetic structure was performed using representation analysis by way of the software SARA*h* [24]. The specific heat, $C_p(T)$, of the samples (2–3 mg pellets) in the range 2–300 K under 0 T and 7 T was measured using the heat pulse method in a commercial physical property measurement system from Quantum Design. The thermal conductivity was measured by pulse-power method using the thermal transport option (TTO) and a Quantum Design DynaCool-9 system. The Raman scattering data were acquired at ambient conditions in backscattering geometry with an alpha 300R WITec system (WITec GmbH, Ulm, Germany). A 532 nm excitation of a frequency-doubled neodymium-doped yttriumaluminum-garnet (Nd:YAG) laser that was restricted to a power output of a few mW, and a 20 X objective lens with a numerical aperture of 0.4 were used. The accumulation of data for each sample consisted of 20 Raman spectra, with each spectrum acquired in 500 milliseconds, for a total time acquisition of 10 seconds. The spectral resolution was 4 cm^{-1}. Appropriate background subtractions were performed for all Raman spectra.

III. COMPUTATIONAL DETAILS

Density functional theory (DFT) calculations were performed to study the electronic and magnetic properties of $CoTa_2O_6$ with the full-potential local-orbital (FPLO) code [17], version 18.00. The exchange and correlation energy considered is the generalized gradient approximation (GGA) in the parametrization of Perdew, Burke, and Ernzerhof (PBE-96) [25]. Self-consistent calculations were carried out using the scalar and four-component full relativistic mode of FPLO. The basis states that were treated as valence states are: Co: 3*s*, 3*p*, 4*s*, 5*s*, 3*d*, 4*d*, 4*p* and Ta: 4*s*, 4*p*, 4*d*, 5*s*, 6*s*, 5*d*, 5*p*, 6*p*, and O: 2*s*, 2*p*, 3*d*. The *k*-space integrations were carried out with the linear tetrahedron method using a $12 \times 12 \times 12k$ mesh in the full Brillouin zone. The convergence criteria for the self consistency cycle were set to be 10^{-8} H for energy convergence and 10^{-6} electronic charge for the charge convergence. The calculations obtained from FPLO were rechecked using the full-potential linearized augmented plane wave (FP-LAPW) method as implemented in the WIEN2k code [26]. The choice of the muffin-tin radii of Co, Ta, and O atoms were taken as 2.07, 2.0, and 1.72 Bohr, respectively.

IV. RESULTS AND DISCUSSION

A. Specific heat

The specific heat curves, $C_p(T)$, of $CoTa_2O_6$ obtained under the application of 0 T, 5 T, and 7 T are presented in

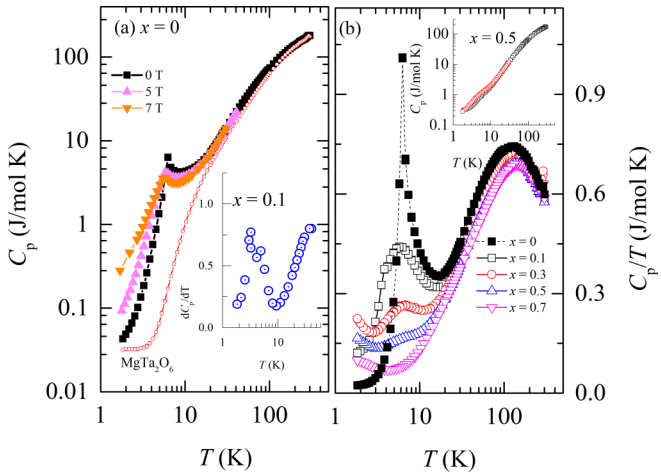

FIG. 2. (a) The specific heat of $CoTa_2O_6$ shows the magnetic phase transition at $T_N = 6.2$ K. The peak at T_N appears robust for 5 T and 7 T. As a lattice analog, the specific heat of $MgTa_2O_6$ is presented in red open circles. dC_p/dT of $x = 0.1$ is shown in the inset. (b) The plot of C_p/T versus T at 0 T for the different compositions of $Co_{1-x}Mg_xTa_2O_6$. The sharp transition in the case of $x = 0$ vanishes upon increasing x. The inset shows the specific heat of $x = 0.5$ in 0 T and 7 T.

Fig. 2(a). The $C_p(T)$ of the nonmagnetic analog compound $MgTa_2O_6$ is plotted in (a) using red open circles. A sharp λ-like transition at $T_N = 6.2$ K is visible for $CoTa_2O_6$. External magnetic fields up to 7 T have a negligible effect on the peak at T_N, however, an enhancement of $C_p(T)$ at $T < T_N$ is noticeable in the presence of externally applied magnetic fields. This may be related to the weak enhancement of ferromagnetism observed previously in $x = 0.7$ [21]. As the Co magnetic lattice is diluted with Mg for $x \geqslant 0.1$, the sharp feature at T_N in $CoTa_2O_6$ is replaced by a broad feature in specific heat. Figure 2(b) shows the plot of $C_p(T)/T$ versus temperature of all $Co_{1-x}Mg_xTa_2O_6$ compositions studied in the present work. It is clear that with increasing Mg content (x), the magnetic transition at T_N is broadened. By taking the derivative, dC_p/dT, we determined the transition temperatures for the $x = 0.1$ and 0.3 compounds. For the $x = 0.1$, anomalies in dC_p/dT are present at 4.9 K and 3.2 K [see the inset of (a)], whereas for the $x = 0.3$ case, it is at 4.5 K. Magnetization results from our previous work on the same composition had shown multiple magnetic anomalies below 28 K in low applied fields which, upon application of external magnetic field, smoothed into a broad transition [21]. The specific heat anomalies (in dC_p/dT) seen in the $x = 0.1$ case match well with our previous magnetization results. In the inset of (b), the $C_p(T)$ of the $x = 0.5$ compound in 0 T and 7 T (red curve) are plotted together. It can be seen that with the application of magnetic field, there is a slight enhancement in the specific heat below T_N. The current specific heat data point towards the presence of ferromagnetic clusters probably of short-range ordered regions that get polarized under the application of an external magnetic field.

In order to obtain the magnetic contribution, $C_m(T)$ towards total specific heat, we subtracted the $C_p(T)$ of $MgTa_2O_6$ from that of $CoTa_2O_6$. Thus obtained $C_m(T)$ of $CoTa_2O_6$ is presented in Fig. 3(a). Earlier studies on $CoTa_2O_6$ have treated the Co atoms as a square net of Ising spins in order to model the experimental specific heat [2]. We find that the model of a square net of spins holds good in the present case as can be seen by the solid line in (a), which is the specific heat of an Ising net of spins. Further, a broad feature is seen at $T > T_N$ reminiscent of a Schottky-type anomaly. An attempt to model it using a two-level Schottky term leads to an acceptable fit as can be seen by the blue solid line in (a). Short-range spin correlations that exist above the transition temperature giving rise to a broad peak in specific heat is reported in $CuSb_2O_6$ for example [13,27]. The characteristic energy scale determined from the Schottky fit in the present case corresponds to $\Delta \approx 260$ K. Another plausible scenario that can support the Schottky-like feature in the specific heat is the orbital magnetism that might be active in $CoTa_2O_6$ [16]. We further obtain support that the Schottky-like peak

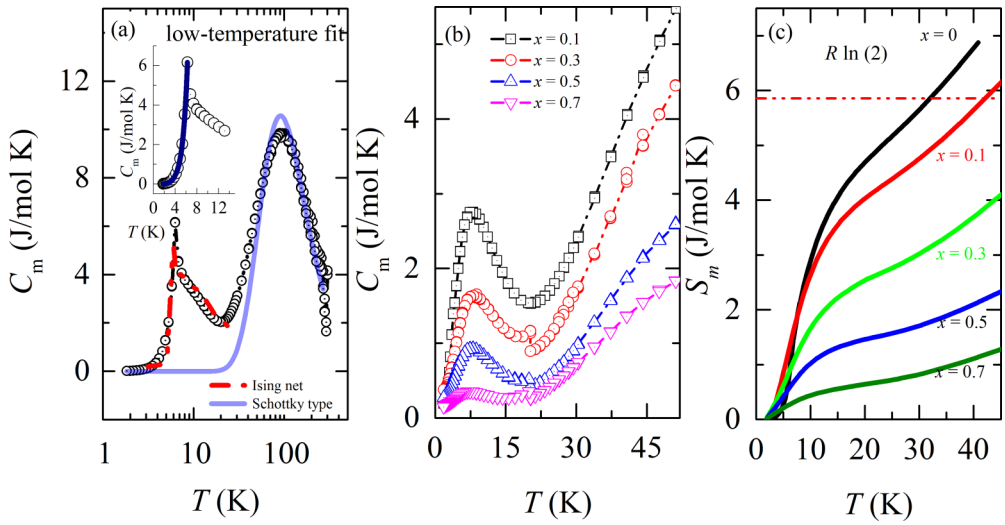

FIG. 3. (a) The magnetic specific heat C_m of $CoTa_2O_6$ (open circles). The red solid line is the specific heat of a square net of Ising spins while the blue line is a fit using a two-level Schottky term. The inset shows the C_m along with a fit using Eq. (1). (b) Shows C_m of $x = 0.1$, 0.3, 0.5, and 0.7. The magnetic entropy, S_m, for $Co_{1-x}Mg_xTa_2O_6$ $x = 0$ to 0.7 are plotted in (c).

TABLE I. The Sommerfeld coefficient and Debye temperature of $Co_{1-x}Mg_xTa_2O_6$ compounds extracted from the analysis of low temperature specific heat.

x	γ (mJ/mol K^2)	β (mJ/mol K^4)	θ_D (K)
0	80.4(1)	0.0241(5)	892
0.1	55.4(3)	0.0254(3)	876
0.3	28.7(3)	0.0299(5)	829
0.5	13.3(7)	0.0191(7)	963
0.7	4.4(1)	0.0211(5)	931

in specific heat is closely linked to the theoretical specific heat of $S = 3/2$ 1D-Ising model. The calculations of specific heat for an $S = 3/2$ 1D-Ising model predicts a peak at $1.25R$ or about 10.4 J/mol-K and should occur at $k_B/J = 2.5$ [28]. This closely matches the value at the top of the 100 K peak of $C_m(T)$ in Fig. 3(a). Further, in the present case, $J/k_B = -40$ K, which might be linked to the interchain exchange constant. Similar Schottky-like features are observed in the $C_m(T)$ of $x = 0.1$–0.7 compositions. This supports the presence of short-range spin correlations in all of the $Co_{1-x}Mg_xTa_2O_6$ series. Progressive Mg doping disrupts the Co chains and leads to the formation of clusters of spins displaying such Schottky-like features in specific heat. The $C_m(T)$ of the other compositions in the $Co_{1-x}Mg_xTa_2O_6$ series are shown in panel (b) of the figure. Evidently, the magnetic contribution to the specific heat decreases with increasing Mg content. The magnetic entropy that is obtained using $S_m = \int_0^T dC_m/T\,dT$ is plotted for all compositions in (c). Only 6% of the total spin-only entropy of $R\ln(2S + 1)$ ($S = 3/2$ and R is the universal gas constant) is released close to the T_N. The low magnetic entropy release observed close to the magnetic ordering temperature indicates that a significant amount of short-range magnetic order exists above the T_N in $CoTa_2O_6$ and the Mg-doped compounds [29].

Further, we have analyzed the low temperature specific heat of $Co_{1-x}Mg_xTa_2O_6$ using the expression, $C_m(T) = \gamma T + \beta T^3$. The fit parameters and the values of Debye temperature estimated for the different compositions are given in Table I. The Debye temperature was estimated using the equation, $\theta_D = (12p\pi^4R/5\beta)$, where p is the number of atoms in the unit cell and R is the universal gas constant. The values of γ show a gradual decrease as a function of composition x, whereas the β values show an anomaly for $x = 0.5$. The value of γ that is observed in $CoTa_2O_6$ lies intermediate with the values of 203 mJ/mol K^2 for $CoSb_2O_6$ and 58.7 mJ/mol K^2 for $CuSb_2O_6$ [29]. The insulating nature of these compounds might point to the fact that the γ term signifies the entropy associated with short-range order. The magnetic specific heat in the temperature range below T_N could be modeled using

$$C_m(T) = \gamma_{AFM}T + A_2\exp(-\Delta/k_BT). \quad (1)$$

The first term on the right-hand side of this expression is the specific heat of free electrons near the Fermi level and the second term originates from the electrons that participate in the magnon dispersion. A fit using the above expression to the experimental magnetic specific heat below T_N leads to the values $\gamma = 0.018(3)$, $A_2 = 0.06(5)$, and $\Delta/kB = 20.2(5)$ K. This fit is presented in the inset of Fig. 3(a) as a thick solid line.

B. Raman scattering and thermal conductivity

For a better understanding of the Mg-doping effects on the structural features of $CoTa_2O_6$, we present in Figs. 4(a)–4(c) the room-temperature micro-Raman spectra of $Co_{1-x}Mg_xTa_2O_6$ with $x = 0$, 0.1, 0.5, 0.7, and 1.0. Although similar Raman vibrational lines for $CoTa_2O_6$ and $MgTa_2O_6$ ($x = 0.0$ and 1.0) have been reported in the literature [30,31], some repetition of results in research contributes to the supportive purposes of cross checking and confirmation of reproducibility. Since the Raman spectra of tantalates are dominated by modes corresponding to Ta_2O_6 units, with the bivalent metal atoms making a much smaller contribution, a comparison between the Raman results presented in Figs. 4(a) and 4(c), indeed, reveals an expected similarity of vibrations [30]. However, definite trends are observed in Fig. 4(b) with Mg atoms progressively substituting for Co atoms and resulting in elongations of Co-O bonds and angle modifications of the cyclic Ta-O-Co-O-Ta structure (as Ta-O bonds will couple differently with Co-O bonds after substitution). Direct evidence of Mg incorporation is the increase in the intensity of the 209 cm^{-1} Raman line, which corresponds to vibrational modes of Mg-O bonds [see the Raman spectrum of $MgTa_2O_6$ in Fig. 4(c)]. Furthermore, frequency shifts and intensity changes are also seen in all $Co_{1-x}Mg_xTa_2O_6$ Raman spectra for other vibrational lines. For example, with Mg doping, the Raman peak at 234 cm^{-1} in the spectrum of $CoTa_2O_6$ [see Fig. 4(a)] increases in intensity and shifts to a higher frequency, to a final value of 242 cm^{-1} in the Raman spectrum of $Co_{0.3}Mg_{0.7}Ta_2O_6$, a value that is very close to the corresponding one seen in the Raman spectrum of $MgTa_2O_6$. The Raman feature at 318 cm^{-1} in the spectrum of $CoTa_2O_6$ shifts to 328 cm^{-1} in the spectrum of $Co_{0.3}Mg_{0.7}Ta_2O_6$. It also exhibits a similar intensity increase. The 386 cm^{-1} Raman line, too, presents higher frequency shifts, to 415 cm^{-1} in the Raman spectrum of $Co_{0.3}Mg_{0.7}Ta_2O_6$; it also decreases in intensity. A similar decrease in intensity is observed for the Raman peak at 465 cm^{-1} without a frequency shift. Comparison of the intensity of this vibrational line in the Raman spectrum of $CoTa_2O_6$ with its intensity in the spectrum of $MgTa_2O_6$ reveals that the observed pattern in intensity changes in the $Co_{1-x}Mg_xTa_2O_6$ Raman spectra again correlates with the amount of Mg doping. The Raman vibrational lines at 234 and 318 cm^{-1} in the $CoTa_2O_6$ spectrum have lower intensities than those at 243 and 328 cm^{-1} in the $MgTa_2O_6$ spectrum. On the other hand, the Raman bands at 386 and 465 cm^{-1} in the $CoTa_2O_6$ spectrum have higher intensities than those at 418 and 465 cm^{-1} in the $MgTa_2O_6$ spectrum. Thus, with more Mg incorporation, the Raman spectra of $Co_{1-x}Mg_xTa_2O_6$ are expected to resemble more that of $MgTa_2O_6$ and less that of $CoTa_2O_6$. Finally, the frequency at 689 cm^{-1} associated with Ta-O bond vibration in the $CoTa_2O_6$ Raman spectrum [Fig. 4(a)] shifts slightly in the $Co_{1-x}Mg_xTa_2O_6$ spectra, to a value of 702 cm^{-1} for the case with the highest amount of Mg doping. Thus, the Raman results obviously demonstrate morphological changes of the $CoTa_2O_6$ structure with Mg doping.

The temperature dependence of thermal conductivity, $\kappa(T)$, measured on the polycrystalline samples of $CoTa_2O_6$, $Co_{0.9}Mg_{0.1}Ta_2O_6$, and $Co_{0.3}Mg_{0.7}Ta_2O_6$ is shown in the main panel of Fig. 4(d). In the inset of the figure, the low

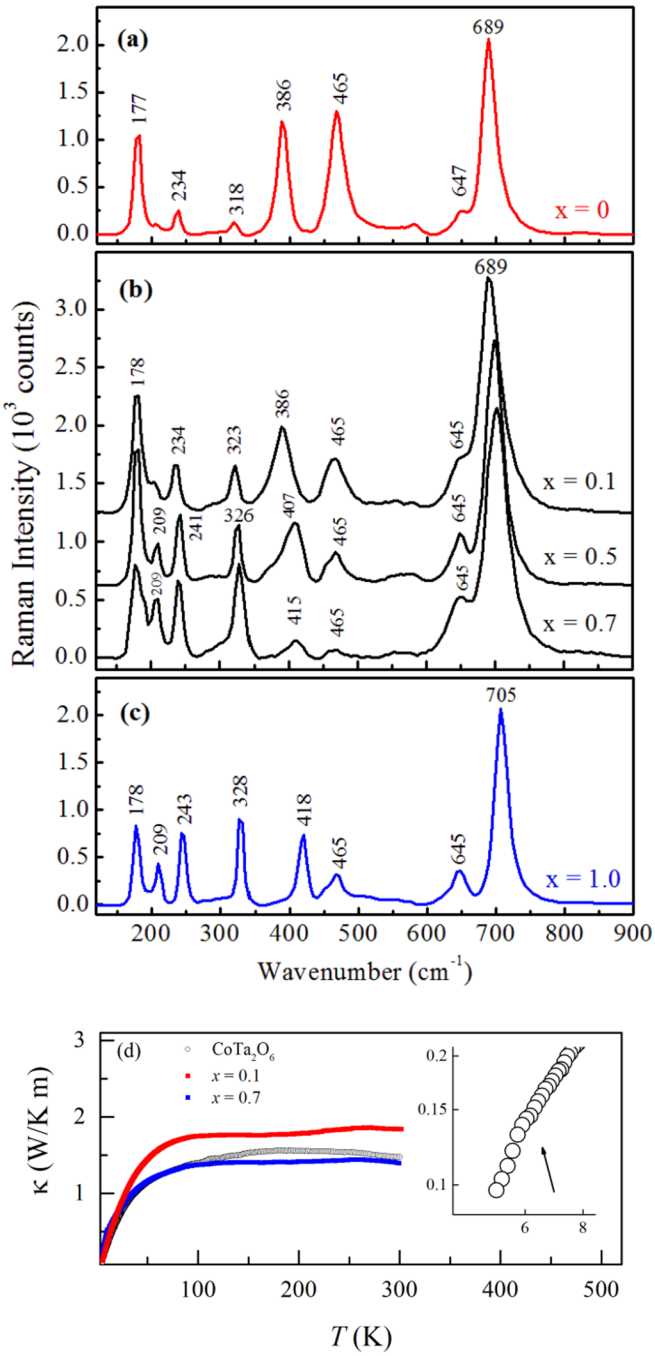

FIG. 4. Raman scattering intensity of $Co_{1-x}Mg_xTa_2O_6$ for (a) $x = 0$, (b) $x = 0.1$, 0.5, 0.7, and (c) $x = 1.0$ at $T = 300$ K. The thermal conductivity $\kappa(T)$ of the three compositions of $Co_{1-x}Mg_xTa_2O_6$: $x = 0$, 0.1, and 0.7. The phase transition at $T_N \approx 6$ K in the case of $x = 0$ is shown enlarged in the inset.

temperature part of $\kappa(T)$ for $CoTa_2O_6$ in the vicinity of the magnetic phase transition $T_N = 6.2$ K is shown. The value for T_N observed in $\kappa(T)$ is similar to the value observed in $C_p(T)$. Recent detailed work on the thermal conductivity of $CoTa_2O_6$ and $CoSb_2O_6$ single crystals showed that the Ta compounds have lower values of $\kappa(T)$ compared to the Sb counterparts [18]. It is worth noting that the thermal conductivity of our $CoTa_2O_6$ sample could be reduced due to the porosity that might be present in the material. Furthermore, a sharp upturn of $\kappa(T)$ is observed in $CoTa_2O_6$ at the Neél temperature. In our polycrystalline sample, this transition is not so sharp as observed in the single crystals but is clearly seen as a kink in the $\kappa(T)$ curve. The thermal conductivity features observed in the present case of $CoTa_2O_6$ confirm the fact that the strong phonon scattering is coupled to the short-range antiferromagnetic order that develops at temperatures above the Neél temperature. $\kappa(T)$ is very low and nearly temperature independent above 100 K. The low value of $\kappa(T)$ probably indicates low charge carrier density and the temperature independent nature reflects very efficient scattering of heat carrying phonons, which might be comparable to phonon-glass systems. Detailed thermal transport studies on single crystals might be helpful to conclude on this topic.

C. Neutron diffraction

The neutron powder diffraction patterns of $Co_{1-x}Mg_xTa_2O_6$ were recorded at the PSD instrument at different temperatures between 295 K and 5 K. Figures 5(a) and 5(b) show the neutron powder diffraction patterns obtained for the $x = 0$ compound (i.e., $CoTa_2O_6$) at 295 K and 5 K, respectively. The crystal structure of $CoTa_2O_6$ is well documented in the literature [32] as a trirutile type of crystal structure. All the compositions of $Co_{1-x}Mg_xTa_2O_6$ in the present study were identified to retain the trirutile space group $P4_2/mnm$ at all temperatures. In Fig. 5, the red circles represent the experimentally recorded pattern while the black solid line is the model fit using $P4_2/mnm$ space group. In the trirutile structure of $CoTa_2O_6$, the Co^{2+} and Ta^{5+} cations are surrounded by O^{2-} octahedra, and successive CoO planes (at $z = 0$ and $z = 1/2$) are separated by two Ta-O planes. The refined Co-O bond distances and the O-Co-O bond angles are given in Table II along with the refined atomic parameters and lattice constants. The refined lattice parameter at $T = 295$ K is comparable to the value reported earlier in a structural report [32]. We did not observe any structural phase transformation in $CoTa_2O_6$ as a function of temperature down to 5 K or as a function of composition x in the case of $Co_{1-x}Mg_xTa_2O_6$. The x dependence of both a and c showed a weak anomaly at $x = 0.5$ (not shown) which was reflected in the bond parameters as well. The most recent report on the neutron diffraction study of $CoTa_2O_6$ reports on a polycrystalline sample with small impurities, CoO and Ta_2O_5 [20]. Though the crystal structure is refined in the $P4_2/mnm$ space group, the lattice constants reported ($a = 4.715(9)$ Å, $c = 9.127(6)$ Å at 1.5 K) are different from the values obtained in the present work.

With the reduction in temperature to 5 K, additional Bragg peaks at $2\theta \approx 11.3°$, 14.2°, 11.3°, 17°, and 19° are observed in the neutron powder diffraction pattern. The additional peaks, that correspond to the magnetic order developing in the compound below the T_N, are shown enlarged in the inset of Fig. 5(b). In order to solve the magnetic structure, a profile fit and k search was performed using the utilities within Fullprof Suite software. A k value of $(\frac{1}{4}, \frac{1}{4}, 0)$ was obtained. Using the representation analysis tool in SARAh, we then obtained the symmetry-allowed magnetic representations for the space

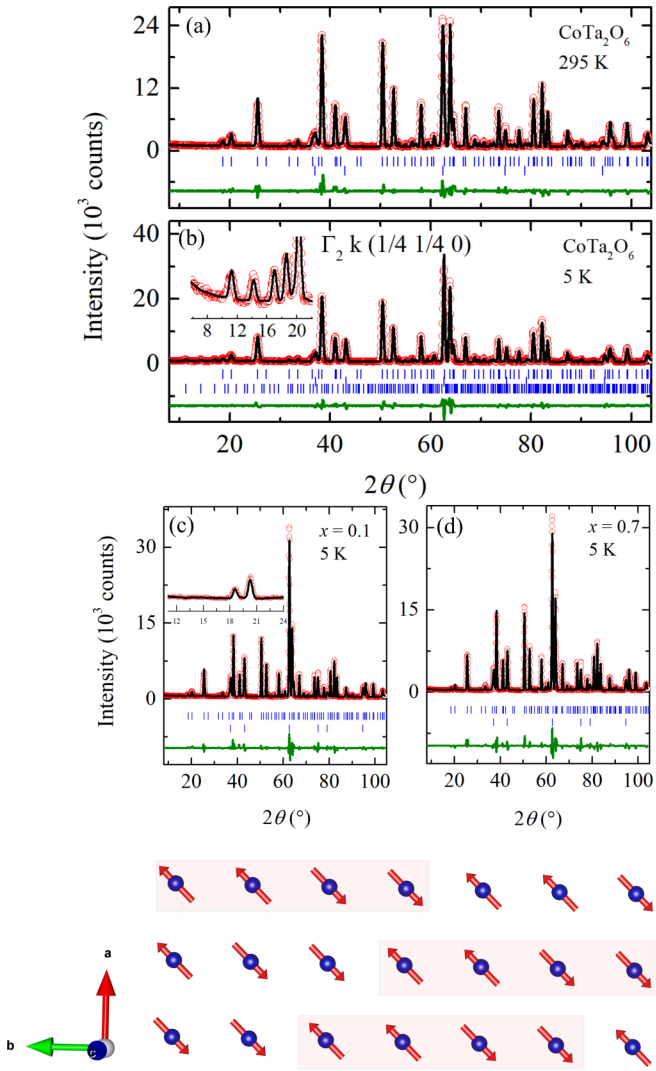

FIG. 5. Top: (a) The neutron powder diffraction pattern of $CoTa_2O_6$ at 295 K refined in the $P4_2/mnm$ space group. (b) Shows the pattern at 5 K where the magnetic peaks are shown magnified in the inset. Γ_2 representation with a propagation vector $(\frac{1}{4}\frac{1}{4}0)$ accounts for the magnetic peaks. Nuclear Bragg peaks from the Al sample holder used for the experiment are accounted for in all cases. (c),(d) Shows the patterns for $x = 0.1$ and 0.7, respectively, at 5 K. Bottom: A representation of a layer of Co magnetic moments in the *ab* plane showing the $(++--)$ arrangement.

group $P4_2/mnm$. Accordingly, the magnetic structure was determined in Γ_2 representation. The Co magnetic moments adopt a magnetic arrangement $(++--)$ that constitutes a sinewave modulated structure. The average magnetic moment on the Co sites is obtained as 2.3(2) μ_B. The magnetic structure presented here is similar to that put forward in the case of weakly diluted $Fe_{1-x}Co_xTa_2O_6$ [19]. The magnetic structure of $FeTa_2O_6$ is described in terms of three-dimensional stacking of antiferromagnetic planes, where the anisotropy of one set of planes is rotated 90° with respect to the other [33]. On the other hand, the magnetic structure of $CoTa_2O_6$ is close to that of a complex helix with components on the base plane and along the *c* axis [3]. Hence a solid solution of $CoTa_2O_6$ and $FeTa_2O_6$ resulted in an antiferromagnetic structure with competing interactions, where intermediate compositions possess two different magnetic propagation vectors. The magnetic structure solution presented here can be connected to the specific heat of $CoTa_2O_6$. The $(\frac{1}{4}, \frac{1}{4}, 0)$ propagation vector leads to a situation where neutron data are not able to differentiate between a sequence $(++--)$, where all magnetic moments are equal, or a situation $(+0\ -\ 0)$ where two out of four spins have a large moment and the other two, no magnetic moment. Hence, the magnetic structure estimated here aligns well with the observation in an earlier work where the specific heat below T_N suggested that a large fraction of spins remained disordered [16].

TABLE II. The structural parameters of $CoTa_2O_6$ at 295 K and 5 K obtained from the refinement of the neutron powder diffraction data are presented in the top two rows. The refined lattice parameters at $T = 295$ K are a (Å) = 4.7382(9), c (Å) = 9.1758(2) and at $T = 5$ K are a (Å) = 4.7421(3) and c (Å) = 9.1791(3). The bond parameters of $Co_{1-x}Mg_xTa_2O_6$ at 295 K as a function of x are presented in the last row of the table.

$T = 295$ K	x (Å)	y (Å)	z (Å)
Co (2*a*)	0	0	0
Ta (4*e*)	0	0	0
O (4*f*)	0.3118	0.3118	0
O (8*j*)	0.2960	0.2960	0.3230
$T = 5$ K	x (Å)	y (Å)	z (Å)
Co (2*a*)	0	0	0
Ta (4*e*)	0	0	0
O (4*f*)	0.3115	0.3115	0
O (8*j*)	0.2957	0.2957	0.3236
x	Co-O1 (Å)	Co-O2 (Å)	O2-Co-O2 (°)
0	2.0815(19)	2.1164(16)	80.52(8)
0.1	2.088(3)	2.1156(17)	80.58(9)
0.3	2.0872(19)	2.1169(16)	80.39(8)
0.5	2.084(3)	2.1104(17)	80.08(9)
0.7	2.078(3)	2.113(3)	79.84(12)

The neutron powder diffraction patterns obtained for $x = 0.1$ and 0.7 at 5 K are presented in Figs. 5(c) and 5(d), respectively. The low-angle region of the pattern is shown magnified in (c) to clearly show that the magnetic Bragg peaks are absent even at Mg dilution of 10%. The temperature dependence of magnetization of $x = 0.1$ composition revealed anomalies at low temperatures [21]. The present results obtained through neutron diffraction confirm that the magnetism in $CoTa_2O_6$ is completely suppressed upon increasing the concentration of Mg to 10%. The neutron diffraction patterns of $x = 0.3$, 0.5, and 0.7 at 295 K and 5 K are similar to that of $x = 0.1$ confirming the absence of long-range magnetic ordering in $Co_{1-x}Mg_xTa_2O_6$ for $x > 0.1$. The current results align well with the bulk magnetization data [21] except for an enhancement of ferromagnetic correlations found in the heavily doped composition ($x = 0.7$), however, in external magnetic fields. We do not observe experimental indications of diffuse magnetic order in any of the $Co_{1-x}Mg_xTa_2O_6$ compositions.

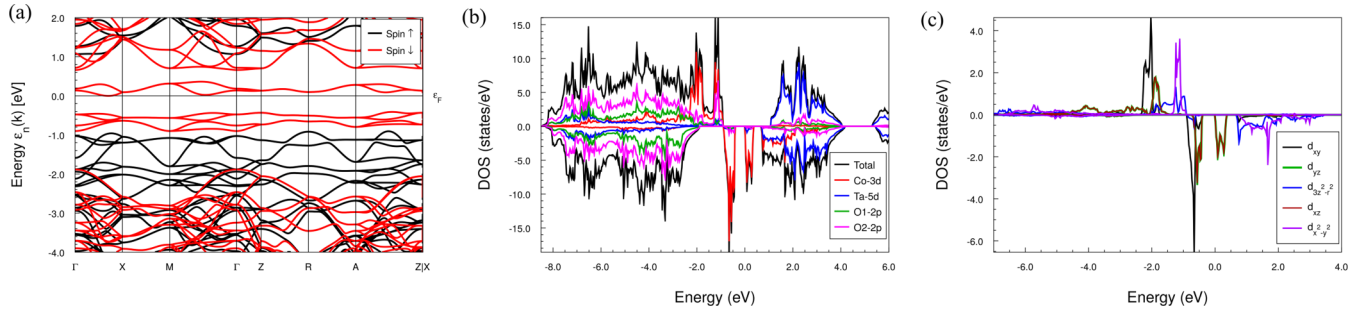

FIG. 6. (a) Scalar-relativistic band structure within GGA for the FM state of $CoTa_2O_6$. Bands in black (red) indicate the spin-up (spin-down) channels. (b) Total (black) and partial DOS for Co (red), Ta (blue), apical-O (green), and planar-O (pink) of $CoTa_2O_6$ within GGA. (c) Orbital resolved DOS for Co-3d states in $CoTa_2O_6$.

D. Density functional theory

We first consider the geometrical optimization for the experimental parameters obtained from our diffraction experiments as tabulated in Table II for $T = 5$ K. All the results presented here are from the relaxed structure. The deviation of the obtained data are negligible (i.e., $\leqslant 2\%$ change in the experimental positions) compared with the experimental lattice parameters. We first consider the electronic properties of a nonmagnetic configuration by DFT calculations, from where we observe a sharp peak at the Fermi level (E_F) indicating the magnetic instability of $CoTa_2O_6$. Based on this, we further investigate the magnetic ground state of $CoTa_2O_6$, using the optimized parameters as mentioned above. The total energy calculations for the collinear ferromagnetic (FM-↑↑), antiferromagnetic (AFM-↑↓), and nonmagnetic (NM) configurations were calculated. The ground state was found to be FM where the energy difference between the lowest total energy state and the first excited AFM state amounts to just 5.77 meV per unit cell. The small energy difference between FM and AFM clearly indicates the competing ground state and the reasonable explanation to the AFM ground state below 5 K as observed here in the experiment. The FM ground state obtained through the DFT calculations is obtained by using the structural parameters reported by some of us recently [21].

We further consider the magnetic anisotropy energy (MAE) of $CoTa_2O_6$ for the FM ground state. The easy axis was found along the (100) direction with MAE of approximately 2.5 meV per unit cell. In the calculations, each Co couples ferromagnetically with its neighbor Co via oxygen and Ta in the trirutile structure. In $CoTa_2O_6$, each Co with charge state $+2$ formally has a $3d^7$ configuration. This is expected to carry a magnetic moment of ± 3 μ_B within an ionic picture, while our first-principles calculation indicates the spin moment of 2.68 μ_B and an orbital moment of 0.17 μ_B per Co. Although finite strength of spin-orbit coupling (SOC) has been observed on the Co site, its influence at and around E_F in the electronic structure is negligible. Because of the charge transfer effects between Co(Ta) and O atoms, Ta and oxygen gain a partial moment of 0.048 μ_B per Ta, 0.032 μ_B per planar oxygen, and 0.041 μ_B per apical oxygen atoms. The difference between two in-equivalent atoms is mainly due to their different bond lengths [Co-O bond length: apical (planar) 2.053 (2.093) Å] arranged with the Co atoms. The obtained moment of Co is found to be in good agreement with our experimental moment of 2.13 μ_B/Co. The small difference is attributed to the environmental effects (temperature, etc.), SOC, and the hybridization among the Ta and oxygen atoms.

We performed the DFT calculations using the crystal parameters obtained at 11 K. This data suggests the FM ground state. Within the GGA calculations, $CoTa_2O_6$ is found to be an indirect band gap semiconductor as shown in Fig. 6(a). The band gap found in the spin-up channel is 2.0 eV, while that in the spin-down channel is ∼0.47 eV, respectively. As observed from the total and partial DOS in Fig. 6(b), the dominant contributions to the total DOS in the spin-up channel at and below E_F (between -2.5 eV to 0.0 eV) are mainly from the Co-3d orbitals hybridizing with the O-2p states [see Fig. 6(b)] while above E_F (<1.5 eV) are the contributions from Ta 5d states. This clearly shows the full occupancy of Co 5d states in the spin-up channel (see also the spin-up band structure below E_F where five d bands are clearly distinct with two degenerate bands overlapping at high symmetry points such as X, M, etc. below -1 eV). In the spin-down channel on the other hand, major contributions below -1.5 eV are from the O 2p states while two occupied d states from Co 3d orbitals are found with sharp peaks between -1 and -0.5 eV hybridizing with the O 2p states, while an isolated d band from the t_{2g} orbitals lies just above the E_F. Due to crystal field effect, the two empty bands from Co $d(e_g)$ lie around 1.3 eV above E_F hybridizing with the Ta-5d orbitals. These features can be observed distinctly from the band structure shown in Fig. 6(a) and the local orbitals from Co 3d states [see Fig. 6(c)]. Since Co^{2+} has five valence electrons occupied in the spin-up and only two t_{2g} states are expected to be occupied in the spin-down channel, the remaining three empty orbitals should lie above the conduction band. The partial DOS result shown in Fig. 6 is found consistent with the idea that the Co $d(t_{2g}^3 e_g^2)$ spin-up channel is fully occupied, lying below -1 eV from the E_F. In the spin-down channel, two of the t_{2g} are occupied close to E_F while one empty t_{2g} and two empty e_g states appear above E_F in the conduction region. The corresponding band structure is shown in Fig. 6(b). As observed, in the scalar relativistic mode (absence of SOC), $CoTa_2O_6$ has a band gap of 2.0 eV in the spin-up channel, while that in the spin-down channel is ∼0.47 eV. In contrast, when SOC is considered, the gap size is reduced to ∼0.41 eV (not shown). The noticeable change is the shifting of E_F from the bottom of the conduction band to the top of the valence band.

The specific heat data presented in this work point towards disordered ferromagnetic spin clusters in $CoTa_2O_6$. The neutron diffraction analysis supports the above scenario where the $(++--)$ or $(+0\ -\ 0)$ structures are indicated. Slight deviation from nominal stoichiometry due to volatility of Co might drive a certain degree of disorder in $CoTa_2O_6$. This may, in turn, influence stabilization of different valences for Co which need to be probed in detail using high resolution x-ray spectroscopy. The vacancies of Co that may have occurred during the synthesis process can indirectly influence oxygen stoichiometry of $CoTa_2O_6$. In such a scenario, we can expect to observe FM similar to carbon-doped ZnO or aluminum-doped TiO_2 thin films [34,35]. Ferromagnetism is expected to be highly favorable in the present case as $CoTa_2O_6$ has already shown magnetism in the absence of vacancies, as per our DFT results. Oxygen vacancy at a particular site can be expected to transfer hole either to Ta or Co site. The vacancy can thus be expected to modify the electronic as well as the magnetic properties of $CoTa_2O_6$ however, a direct correlation of such results do not exist as of now. Single crystals of another trirutile, $MgTa_2O_6$, prepared using the technique of optical floating zone under argon, was reported as appearing black due to oxygen vacancies [36]. However, synthesis in air helps in achieving a yellow color for the crystal with less oxygen vacancies [37]. The intrinsic atomic defects due to oxygen off-stoichiometry in trirutiles has been recently treated using detailed simulations [38]. The oxygen positions in the trirutile structure has two Wyckoff positions and the most favorable energy is associated with the vacancies on the O1 site. However, the calculated defect energies suggested that they are insignificant in the case of $MgTa_2O_6$. In $CoTa_2O_6$, similarly, we do not anticipate significant changes in the magnetic properties due to slight alterations from nominal stoichiometry.

V. CONCLUSIONS

Signatures of low dimensionality and short-range magnetic order are observed in the trirutile series, $Co_{1-x}Mg_xTa_2O_6$. The specific heat of $CoTa_2O_6$ reveals a magnetic phase transition at 6.2 K and a broad feature at $T > T_N$, ascribed to short-range magnetic order. The T_N is relatively robust in applied magnetic fields but is reduced upon Mg doping at the Co site. However, the broad feature related to short-range spin order is present in all of the doped compositions. A low value of entropy is released at T_N. Analysis of specific heat supports low-dimensional features of magnetism and short-range order in $Co_{1-x}Mg_xTa_2O_6$ trirutiles. Mg doping of 10% is sufficient to destabilize the antiferromagnetic order seen in $CoTa_2O_6$. Performing neutron diffraction on a phase-pure sample, we have determined the magnetic structure of $CoTa_2O_6$ to be a sine wave-type order with propagation vector k $(\frac{1}{4}, \frac{1}{4}, 0)$. Density functional theory studies predict the ferromagnetic ground state, however, the negligible (small) total energy differences between the ferromagnetic and antiferromagnetic configuration indicates a competing ground magnetic state. This in turn supports the short-range order we observe in specific heat data. Our computational results supports the observation of strong anisotropy effects in the class of trirutile compounds.

ACKNOWLEDGMENTS

H.S.N. acknowledges the UTEP start-ups and the Rising-STAR award from UT system in supporting this work. K.G. acknowledges support from the DOEs Early Career Research Program. N.P. acknowledges support from INL's LDRD program (18P37-008FP). M.P.G. acknowledges the Alexander von Humboldt Foundation, Germany for the financial support, and Higher Education Reform Project of Tribhuvan University for the start-up grant. M.P.G. also thanks Ulrike Nitzsche for technical assistance. B.P.B. thanks Sainamaina-Municipality, Nepal for the partial support, and S.B. thanks UGC-Nepal for the scholarship support under the MRS-2075/76 program. A.M.S. thanks the SA NRF (93549) and the URC/FRC of UJ for financial assistance.

[1] M. Takano and T. Takada, Mater. Res. Bull. **5**, 449 (1970).
[2] R. K. Kremer, J. E. Greedan, E. Gmelin, W. Dai, M. A. White, S. M. Eicher, and K. J. Lushington, J. de Phys. Colloq. **49**, C8 (1988).
[3] J. N. Reimers, J. E. Greedan, C. V. Stager, and R. Kremer, J. Solid State Chem. **83**, 20 (1989).
[4] M. Whangbo, H. Koo, and D. Dai, Inorg. Chem. **42**, 3898 (2003).
[5] F. Haldane, J. Phys. C: Solid State Phys. **14**, 2585 (1981).
[6] D. Dmitriev, JETP Lett. **80**, 303 (2004).
[7] D. V. Dmitriev and V. Y. Krivnov, Phys. Rev. B **70**, 144414 (2004).
[8] J. Kurmann, J. Appl. Phys. **52**, 1968 (1981).
[9] J. Kurmann, Physica A **112**, 235 (1982).
[10] J. M. Law, H.-J. Koo, M.-H. Whangbo, E. Brücher, V. Pomjakushin, and R. K. Kremer, Phys. Rev. B **89**, 014423 (2014).
[11] M. Kato, A. Hatazaki, K. Yoshimura, and K. Kosuge, Physica B **281**, 663 (2000).
[12] A. B. Christian, S. H. Masunaga, A. T. Schye, A. Rebello, J. J. Neumeier, and Y.-K. Yu, Phys. Rev. B **90**, 224423 (2014).
[13] A. Rebello, M. G. Smith, J. J. Neumeier, B. D. White, and Y.-K. Yu, Phys. Rev. B **87**, 224427 (2013).
[14] D. Kasinathan, K. Koepernik, and H. Rosner, Phys. Rev. Lett. **100**, 237202 (2008).
[15] A. B. Christian, C. D. Hunt, and J. J. Neumeier, Phys. Rev. B **96**, 024433 (2017).
[16] A. B. Christian, A. T. Schye, K. O. White, and J. J. Neumeier, J. Phys.: Condens. Matter **30**, 195803 (2018).
[17] K. Koepernik and H. Eschrig, Phys. Rev. B **59**, 1743 (1999).
[18] N. Prasai, A. B. Christian, J. J. Neumeier, and J. L. Cohn, Phys. Rev. B **98**, 134449 (2018).
[19] E. J. Kinast, V. Antonietti, D. Schmitt, O. Isnard, J. B. M. da Cunha, M. A. Gusmão, and C. A. dos Santos, Phys. Rev. Lett. **91**, 197208 (2003).

[20] E. J. Kinast, C. A. Dos Santos, D. Schmitt, O. Isnard, M. A. Gusmao, and J. B. M. da Cunha, J. Alloys and Comp. **491**, 41 (2010).
[21] R. Baral, H. S. Fierro, L. M. Martinez, S. R. Singamaneni, and H. S. Nair, J. Appl. Phys. **125**, 033904 (2019).
[22] J. Rodriguez-Carvajal, Fullprof Suite, http://www.ill.eu/sites/fullprof/ (2017).
[23] H. M. Rietveld, J. Appl. Crystall. **2**, 65 (1969).
[24] A. S. Wills, Physica B **276**, 680 (2000).
[25] J. P. Perdew, K. Burke, and Y. Wang, Phys. Rev. B **54**, 16533 (1996).
[26] P. Blaha, K. Schwarz, G. K. H. Madsen, D. Kvasnicka, and J. Luitz, An augmented plane wave+ local orbitals program for calculating crystal properties (2001).
[27] A. Nakua, H. Yun, J. N. Reimers, J. E. Greedan, and C. V. Stager, J. Solid State Chem. **91**, 105 (1991).
[28] T. Obakata and T. Oguchi, J. Physical Soc. Jpn. **25**, 322 (1968).
[29] A. B. Christian, A. Rebello, M. G. Smith, and J. J. Neumeier, Phys. Rev. B **92**, 174425 (2015).
[30] E. Husson, Y. Repelin, H. Brusset, and A. Cerez, Spectrochim. Acta A **35**, 1177 (1979).
[31] H. Haeuseler, Spectrochim. Acta A **37**, 487 (1981).
[32] V. Antonietti, E. J. Kinast, L. I. Zawislak, J. B. M. da Cunha, and C. A. dos Santos, J. Phys. Chem. Solids **62**, 1239 (2001).
[33] S. Eicher, J. Greedan, and K. Lushington, J. Solid State Chem. **62**, 220 (1986).
[34] H. Pan, J. B. Yi, L. Shen, R. Q. Wu, J. H. Yang, J. Y. Lin, Y. P. Feng, J. Ding, L. H. Van, and J. H. Yin, Phys. Rev. Lett. **99**, 127201 (2007).
[35] X. Wang, Y. Song, L. L. Tao, J. F. Feng, Y. Sui, J. Tang, B. Song, Y. Wang, Y. Wang, Y. Zhang *et al.*, Appl. Phys. Lett. **105**, 262402 (2014).
[36] M. Higuchi, K. Ando, J. Takahashi, and K. Kodaira, J. Ceramic Soc. Jpn. **101**, 118 (1993).
[37] D. Xu, S. Gao, W. Liu, Y. Liu, Q. Zhou, L. Li, T. Cui, and H. Yuan, RSC Adv. **9**, 839 (2019).
[38] C. Tealdi, M. S. Islam, L. Malavasi, and G. Flor, J. Solid State Chem. **177**, 4359 (2004).